



Full length article



Effects of disorder on the magnetic properties of the Heusler alloy V_2FeAl

R. Smith^{a,*}, Z. Gercsi^a, R. Zhang^{a,b}, K.E. Siewierska^c, K. Rode^a, J.M.D. Coey^a

^a School of Physics, The University of Dublin Trinity College, College Green, Dublin 2, D02 K8N4, Ireland

^b Northwest Institute for Nonferrous Metal Research, Xi'An 710016, China

^c Helmholtz-Zentrum Berlin für Materialien und Energie, Germany

ARTICLE INFO

Keywords:

Heusler alloys
Order–disorder phenomena
Processing
Sputter deposition
Magnetic thin films

ABSTRACT

Magnetic properties of multicomponent alloys depend sensitively on the degree of atomic order on the different crystallographic sites. Here we report the contrast between the magnetic properties of bulk and thin-film samples of the Heusler alloy V_2FeAl . Arc-melted bulk ingots show no site preference of the elements (A2 structure), whereas magnetron-sputtered thin-film samples display a degree of atomic ordering with a tendency towards XA-type order. Electronic structure calculations favour ferrimagnetic XA-type order, and the effect of different pairwise atomic disorder on the element specific and net magnetic moments are evaluated to reproduce experimental observations. XA-type thin-films with iron moment of $1.24 \mu_B$ determined by X-ray magnetic circular dichroism are in agreement with calculation, but the measured net moment of $1.0 \mu_B$ per formula unit and average vanadium moment are smaller than expected from calculations. The measured Curie temperature is approximately 500 K. Films with a higher degree of disorder have a lower T_C , close to 300 K, with a net moment of only $0.1 \mu_B$ at low temperature. The large calculated vanadium moments are destroyed by partial disorder on $4d$ vanadium sites. By contrast, the arc-melted and annealed bulk alloy with a fully-disordered A2 structure shows no spontaneous magnetization at any temperature; it is a Pauli paramagnet with dimensionless susceptibility $\chi_v = 2.95 \times 10^{-4}$.

1. Introduction

Heusler alloys are materials with formula X_2YZ (where X and Y are transition metals and Z is a p-block element); they comprise of four interpenetrating face-centred cubic lattices [1]. The Heusler family is vast, with thousands of possible combinations, and over 800 papers are published on Heusler alloys every year. The family exhibit a wide variety of mechanical, electronic, and magnetic properties, and have applications in many areas of condensed matter physics ranging from spintronics [2,3] to thermoelectric power generation [4] and shape-memory behaviour [5]. The growing global demand for cobalt has driven a recent focus on cobalt-free magnetic Heusler alloys, which aside from economic and environmental concerns, offer advantages for certain spintronics applications, such as reduced magnetization and high coercive fields with the goal of achieving faster dynamics for current-induced magnetization switching for example. The magnetic and transport properties of these materials are highly dependent upon the crystal structure and symmetry, as well as the degree of atomic disorder. Here we contrast the structural and magnetic properties of V_2FeAl in bulk and thin-film form; full Heusler alloys can adopt one of two possible fully-ordered crystal structures, $L2_1$ and XA-type, presented in Fig. 1, as well as many partially-ordered variants depending the processing conditions.

In the $L2_1$ -type crystal structure all of the vanadium atoms occupy the crystallographically equivalent $8c$ Wyckoff sites, with the iron and aluminium on the $4b$ and $4a$ sites respectively. The $L2_1$ structure has space group $Fm\bar{3}m$ (No. 225), with corresponding centrosymmetric point group symmetry $m\bar{3}m$. Alternatively, in the XA-type structure, the vanadium atoms occupy two crystallographically inequivalent Wyckoff positions, $4b$ and $4d$, the iron now on the $4c$ sites and aluminium remains on the $4a$ sites. This structure has space group $F\bar{4}3m$ (No. 216), with corresponding non-centrosymmetric point group symmetry $\bar{4}3m$. As the vanadium atoms in the XA-type crystal structure occupy two crystallographically inequivalent sites, they form two inequivalent magnetic sublattices. $L2_1$ and XA-type are the two fully-ordered crystal structures of V_2FeAl , but there are possible partially-disordered structures listed below and summarized in Table 1;

1. B32 structure in which there is partial disorder between the aluminium atoms in the $4a$ sites and the vanadium atoms in the $4b$ and $4d$ sites.
2. DO_3 structure in which there is partial disorder between the iron atoms in the $4c$ sites and the vanadium atoms in the $4b$ and $4d$ sites.

* Corresponding author.

E-mail address: rsmith1@tcd.ie (R. Smith).

<https://doi.org/10.1016/j.actamat.2024.119733>

Received 22 September 2023; Received in revised form 30 January 2024; Accepted 4 February 2024

Available online 8 February 2024

1359-6454/© 2024 The Authors. Published by Elsevier Ltd on behalf of Acta Materialia Inc. This is an open access article under the CC BY license (<http://creativecommons.org/licenses/by/4.0/>).

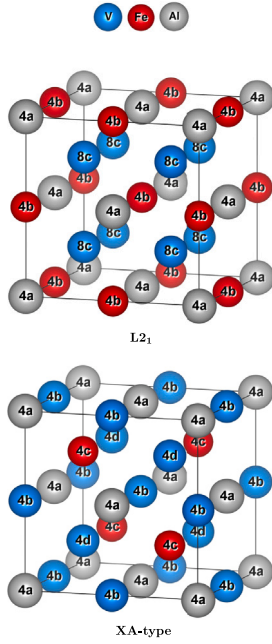


Fig. 1. The two possible fully-ordered crystal structures of V_2FeAl ; $L2_1$ (top) where the vanadium, iron, and aluminium atoms sit in the $8c$, $4b$, and $4a$ Wyckoff sites respectively, and XA-type (bottom) where the iron and aluminium occupy the $4c$ and $4a$ sites respectively and the vanadium atoms sit in $4b$ and $4d$ sites.

Table 1

The possible ordered and disordered structures of V_2FeAl where \leftrightarrow represents disorder between elements in a given site, space group number presented in parentheses.

Struct.	Space group	Disorder
XA	$F\bar{4}3m$ (216)	Fully-Ordered
$L2_1$	$Fm\bar{3}m$ (225)	Fully-Ordered
DO_3	$Fm\bar{3}m$ (225)	$V^{4d} \leftrightarrow Fe^{4c}$
B32	$Fd\bar{3}m$ (227)	$V^{4b,4d} \leftrightarrow Al^{4a}$
B2	$Pm\bar{3}m$ (221)	$Fe^{4c} \leftrightarrow Al^{4a}$
A2	$Im\bar{3}m$ (229)	$V^{4b,4d} \leftrightarrow Fe^{4c} \leftrightarrow Al^{4a}$

- B2 structure in which there is partial disorder between the iron in the $4c$ sites and the aluminium in the $4a$ sites.
- A2 structure is where atoms in all atomic sites are fully disordered.

Whereas these partially and fully-disordered crystal structures can and do form in reality, it is difficult to account for them in electronic structure calculations as the supercells required can become prohibitively large. A recent experimental synthesis of bulk V_2FeAl was reported by Goraus et al. [6], who claim that arc-melted ingots of V_2FeAl are a mixture of $L2_1$ and XA-type structure in a ratio of approximately 3:1. The $L2_1$ and XA structures were found to have cubic lattice parameters of $5.9470 \pm 0.0005 \text{ \AA}$ and $6.0 \pm 0.2 \text{ \AA}$ respectively. However, their bulk X-ray diffraction pattern is missing all of the superlattice reflection characteristic these ordered structures. Our bulk X-ray diffraction pattern matches theirs, but it means that the structure is in fact fully-disordered A2-type. Besides this single experimental measurement, a number of electronic structure calculations have been published on the material. Watson et al. [7] assign V_2FeAl to the $L2_1$ structure and reported a cubic lattice parameter of 583.9 pm with ferrimagnetic ordering. They conclude that the system is unstable due to a low heat of formation of -0.02 eV . Kumar et al. [8] also assigned V_2FeAl to the $L2_1$ structure and found that ferrimagnetic ordering is preferred. On the contrary, Zhang et al. [9] and Skafitourous et al. [10] both found the XA-type structure to be energetically preferred, but also predicted ferrimagnetism to be the magnetic ordering. Published electronic structure calculation results are summarized in Table 2.

The similar X-ray scattering cross-sections of iron and vanadium make it difficult to determine the crystal structure by diffraction alone. It is therefore necessary to rely on other physical properties such as total and element-specific magnetic moments to help infer the crystal structure. Furthermore, X-ray magnetic circular dichroism (XMCD) measurements are utilized to determine the magnetic moment of the iron atoms, and in conjunction with SQUID magnetometry, deduce the vanadium moments.

2. Experimental

Epitaxial thin-films of V_2FeAl were grown by DC magnetron sputtering on $10 \text{ mm} \times 10 \text{ mm}$ single-crystal $MgO(001)$ substrates in the ultra-high vacuum Trifolium Dubium sputtering system with a base pressure less than $1 \times 10^{-9} \text{ mbar}$. The films were co-sputtered from high-purity 50 mm targets of vanadium and binary iron-aluminium (50:50) with a confocal sputtering geometry. Films were grown at a range of deposition temperatures from $300 \text{ }^\circ\text{C}$ to $700 \text{ }^\circ\text{C}$. The MgO substrates were degassed for 1 h at $600 \text{ }^\circ\text{C}$ to reduce surface contamination and encourage epitaxial film growth. Deposition rates were calculated based upon the thicknesses and densities of V and FeAl calibration samples measured by X-ray reflectivity. Following sample deposition, the thin-films were moved under ultra-high vacuum to the system's dedicated *in-situ* X-ray photoelectron spectroscopy chamber equipped with a Specs PHOIBOS 150 hemispherical energy analyser and monochromated Al $K_{\alpha 1}$ X-ray source. The analyser was set to transmission mode with an acceptance area determined by the X-ray spot size (2 mm); all spectra were captured with a pass energy of 10 eV, step size of 0.1 eV, and dwell time of 1 s. Fitting of XPS spectra was carried out using the CasaXPS software package in order to confirm the chemical composition of the films and check for contamination. A fluorescent RHEED screen was used to probe surface crystallinity. A 2 nm capping layer of Al_2O_3 was then deposited *in-situ* by radio-frequency magnetron sputtering to protect the sample against oxidation. Bulk ingots were prepared by arc-melting high-purity elemental samples of vanadium, iron, and aluminium followed by grinding the ingot into a powder and annealing at temperatures ranging from $600 \text{ }^\circ\text{C}$ to $900 \text{ }^\circ\text{C}$.

A Panalytical X'Pert Pro X-ray diffractometer using unmonochromated $Cu K_{\alpha}$ radiation was used to capture diffraction patterns of both bulk powder and thin-film samples. Low-angle X-ray reflectivity was also measured on the thin-films, and the open source GenX XRR refinement programme [11] was used to fit the measured data and determine sample density, thickness, and roughness. Roughness was confirmed by atomic force microscopy (Veeco Nanoscope III atomic force microscope with Multimode software suite). Reciprocal space mapping of the thin-film samples were performed on a Bruker D8 Discover high-resolution X-ray diffractometer with a $Cu K_{\alpha 1}$ beam from a double-bounce $Ge(220)$ monochromator. Rietveld refinement of the powder diffraction patterns was carried out using FullProf [12].

Magnetization measurements were performed with a 5 T Quantum Design MPMS-XL SQUID magnetometer. A 57.2 mg sample of bulk powder was measured, as were thin-films with the field applied perpendicular to the film plane. The diamagnetic contribution from the MgO substrate was corrected for, including a paramagnetic contribution from Mn^{2+}/Fe^{3+} impurities in the MgO which appears below about 100 K [13]. A model consisting of a Curie-Weiss law paramagnetic component (m_{para}), a diamagnetic component (m_{Dia}), and a spontaneous magnetic moment arising from the V_2FeAl thin-film (m_{Sample}) was used to fit magnetization curves at 5 K, 100 K, and 300 K as well as temperature scans in 2 T to ensure the sample was saturated. The paramagnetism in the samples is modelled using a Brillouin function;

$$m_{para} = ng\mu_B J \left[\frac{2J+1}{2J} \coth\left(\frac{2J+1}{2J} \cdot x\right) + \frac{1}{2J} \coth\left(\frac{x}{2J}\right) \right], \quad (1)$$

$$\text{where } x = \frac{g\mu_B J}{k_B(T - \theta_p)} \cdot \mu_0 H_{Applied},$$

Table 2

Results of density functional theory calculations from different works with the preferred structure, magnetic ordering, cubic lattice parameter (pm), element specific moments (μ_B), and total moment (μ_B per unit cell).

Reference	Structure	Magnetic-Ordering	Lattice constant	μ_{Fe}	μ_V	μ_{Al}	$\mu_{Tot.}$
Watson et al. [7]	L2 ₁	FiM	583.9	1.15	-0.19	0.00	0.77
Kumar et al. ^a [8]	L2 ₁	FiM	597.8	1.91	-0.57	0.00	0.46
Skaftouros et al. [10]	XA	FiM	593.0	1.20	2.11	-0.31	2.92
Zhang et al. [9]	XA	FiM	592.0	1.18	2.46	-0.46	3.00

^a Element specific moments add up to 0.77 μ_B , not 0.46 μ_B .

with $J = \frac{5}{2}$. We then refine the number of paramagnetic ions (n), and the paramagnetic Curie temperature (θ_p), to account for magnetic interactions between the ions (the magnitude of this effect is typically less than 1 K). The diamagnetic substrate contribution is simply;

$$m_{Dia} = \chi_V \cdot H_{Applied}, \quad (2)$$

where $\chi_V \leq 0$ is the diamagnetic susceptibility which we refine, ensuring the value does not differ appreciably from values cited in literature. Finally, the temperature dependence of the magnetization is modelled using Bloch's $T^{3/2}$ law;

$$m_{Ferro} = m_0 \left[1 - \left(\frac{T}{T_C} \right)^{3/2} \right], \quad (3)$$

where we fit the spontaneous magnetization at zero temperature (m_0), and the Curie temperature (T_C). Note that 3σ noise removal has been performed on the magnetometry data.

Iron L-edge X-ray absorption near-edge structure (XANES) and X-ray magnetic dichroism (XMCD) of V_2FeAl thin-films were measured at the VEK MAG beamline of the BESSY II light source at Helmholtz-Zentrum Berlin. Measurements were performed on two samples, one ordered and the other disordered. The XANES of the Fe-L_{III} and Fe-L_{II} edges were measured over an energy range of 680 eV to 780 eV in an applied field of 2 T. The absorption is measured in total electron yield, whereby a drain current from the sample is measured, and normalized to a mirror current from the final optical component along the beampath before the sample (this mirror should not show any absorption and the mirror current should therefore be directly proportional to the intensity of incident X-rays). An absorption spectrum is first measured on the VEK MAG beamline using right circularly polarised (RCP) X-rays and an applied magnetic field parallel to the k-vector of the X-rays, the helicity of the X-rays is then reversed (i.e. left circularly polarised (LCP) X-rays are used) and another absorption spectrum is measured in the same applied field. The applied field direction is then reversed such that it is antiparallel to the k-vector of the X-rays and an absorption spectrum is measured with LCP X-rays. The helicity is switched again to RCP X-rays and a final absorption spectrum is measured in the same applied field as the previous spectrum. We calculate the XMCD as the average of the difference between the first and second, and the third and fourth, respectively. By symmetry, the magnetic contribution to dichroism for first and third spectra should be identical, as should the magnetic dichroism of the second and fourth spectra. A background function is subtracted from the XANES spectra prior to analysis. This function consists of a component linear in energy with a pair of arctangent functions at the L_{III} and L_{II} edges, the amplitude of the latter being half that of the former. The integrated areas of the XANES and XMCD spectra are then calculated and the spin and orbital moments deduced using the XMCD sum rules [14]. The moments must be scaled to the number of holes in the 3d band. In this work we chose a value of $n_h = 3.3$, based upon electronic structure calculations of the XA-type structure for the ordered thin-film sample. The number of holes for the disordered sample was then determined by comparing the magnitude of the edge-jumps against the ordered sample and then scaling the value of n_h accordingly. The number of holes in the disordered sample was determined to be approximately half that of the ordered sample.

Thin-film samples were patterned photolithographically into Hall bars with length and width of 50 μm and 10 μm respectively. Ru/Ta/Pt

Table 3

Results of density functional theory calculations for the possible fully-ordered structures and magnetic-ordering of V_2FeAl , showing the cubic lattice parameters (pm), element specific moments (μ_B), and total moments (μ_B per formula unit).

Struct.	Ord.	a	μ_{Fe}	μ_V	μ_{Al}	$\mu_{Tot.}$
L2 ₁	NM	593.5	-	-	-	-
L2 ₁	FM	602.3	1.90	0.20	0.00	2.30
L2 ₁	FiM	602.3	2.10	-0.86	-0.07	0.31
XA	NM	590.6	-	-	-	-
XA	FiM	595.0	1.26	1.88	-0.29	0.05

contact pads were fabricated by a lift-off technique, which were subsequently cold-welded to 50 μm diameter silver wire using high purity indium. Anomalous Hall effect measurements were carried out using a 5.5 T superconducting magnet with a cryostat capable of reaching temperatures down to 10 K. Transport measurements were performed with a DC current of 0.5 mA.

Ab-initio calculations based on density functional theory were carried out using norm-conserving pseudopotentials and pseudo-atomic localized basis functions implemented in the OpenMX software package [15]. The generalized gradient approximation (GGA-PBE) [16] was used for all calculations. We used a 16 atom convenient cell for the cubic structure using $15 \times 15 \times 15$ k-points to evaluate the total energies of the ordered and site-disordered structures. Pre-generated fully relativistic pseudopotentials and the pseudo-atomic orbitals with a typical cut-off radius of 7 atomic units (a.u.) with $s_3p_3d_3$ were used for all elements, respectively. An energy cut-off of 300 Ry was used for the numerical integrations. The convergence criterion for the energy minimization procedure was set to 10^{-7} Hartree. Spin-orbit interaction (SOI) was turned off and only collinear spin configurations were considered.

3. Results

The results of density functional theory calculations performed for different crystal structures and magnetic-orderings of V_2FeAl are shown in Table 3. Fig. 2(a) shows that the XA-type structure is energetically favourable compared to the L2₁ structure, and that ferrimagnetic (FiM) ordering is preferred over non-magnetic or ferromagnetic ordering in both cases. The calculation of the XA-type structure with ferromagnetic ordering did not converge suggesting that the spin configuration is highly unfavourable. The results for FiM XA-type V_2FeAl agree with the previous reports by Skaftouros et al. [10] and Zhang et al. [9], with a slightly larger cubic lattice parameter of 595.0 pm, a slightly higher moment on the iron atoms, and lower moment on the vanadium. The L2₁ results predict a larger lattice parameter than Kumar et al. [8], with higher element specific moments, but a lower net moment. In this structure, the iron atoms in the 4b sites take on a moment of 2.10 μ_B which is mostly cancelled by the antiferromagnetically coupled vanadium moments (-0.86 μ_B) in the 8c sites, giving a small net moment of 0.31 μ_B per unit cell. In the XA-type structure, the Fe atoms occupy the 4c site previously taken by V, showing a smaller moment of 1.26 μ_B . The vanadium atoms remaining in the 4d sites take on a large moment of 1.88 μ_B coupled ferromagnetically to the Fe moment with the remaining vanadium in the 4b sites having a small negative moment of -0.29 μ_B . This gives the XA-type structure a total moment of 2.90 μ_B

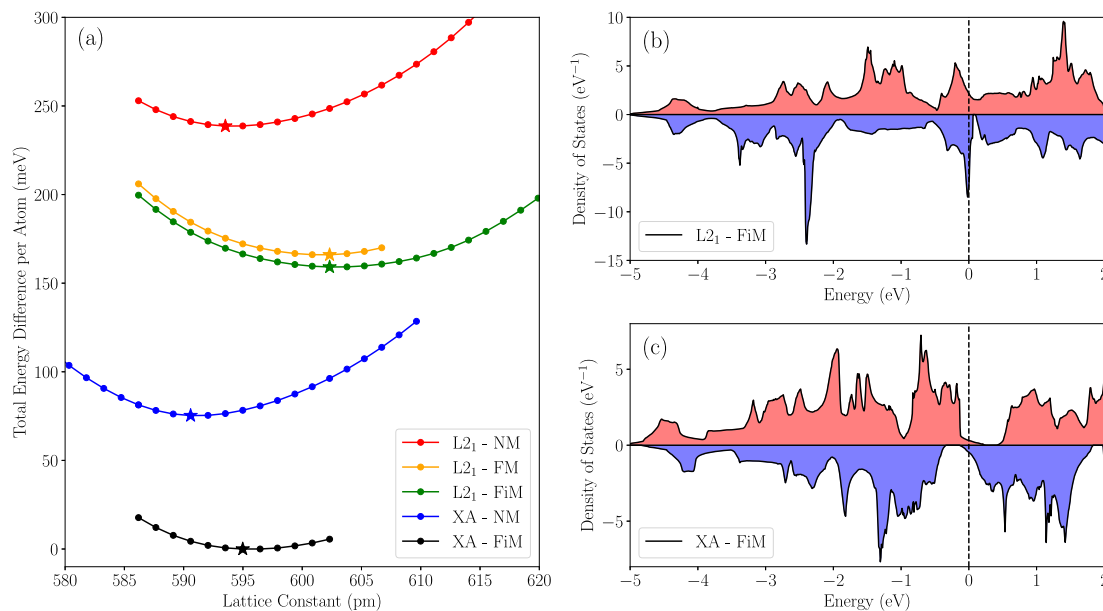


Fig. 2. (a) Total energy difference among the different structures and magnetic order of V_2FeAl as a function of lattice parameter calculated by density functional theory; the star markers represent the lattice constant corresponding to the lowest total energy (b) Density of states for $L2_1$ structured V_2FeAl with ferrimagnetic ordering, (c) Density of states for XA V_2FeAl with ferrimagnetic ordering.

Table 4

Effects of disorder on the magnetic moments of V_2FeAl , element specific moments are in μ_B per atom, total moment is in μ_B per formula unit.

Structural ordering	μ_{Fe}		μ_{Fe}^{avg}	μ_{V_i}		$\mu_{V_i}^{avg}$	$\mu_{V_{II}}$	μ_{Al}	$\mu_{Tot.}$
	(4b)	(4c)		(4b)	(4c)				
100% XA	–	1.26	1.26	–0.29	–	–0.29	1.88	0.05	2.90
75% XA/25% $L2_1$	1.98	1.64	1.73	–0.35	–0.51	–0.39	1.47	0.00	2.81
50% XA/50% $L2_1$	2.02	1.87	1.95	–0.26	–0.46	–0.36	0.99	–0.02	2.56
25% XA/75% $L2_1$	2.16	0.20	1.67	0.16	–0.49	–0.33	–1.07	–0.07	0.20
100% $L2_1$	2.10	–	2.10	–	–0.86	–0.86	–0.86	–0.07	0.31

per formula unit, which matches the moment of $3 \mu_B$ predicted by the Slater-Pauling rule (V_2FeAl has 21 valence electrons $\Rightarrow M = 24 - Z = 3 \mu_B$). Fig. 2(b) and (c) show the calculated density of states of the fully-ordered $L2_1$ and XA-type ferrimagnetic configurations of V_2FeAl . The $L2_1$ structure shows a small gap in the majority states slightly above the Fermi level, whereas the XA-type structure shows gaps in both the majority and minority states with a very low density of states close to the Fermi level. Small changes from the idealized XA-type structure could result in a change of band structure resulting in the formation of a type-II spin-gapless semiconductor where one spin channel shows a finite bandgap and the other shows a gap close to zero [17].

The effects of binary disorder on the magnetic properties of V_2FeAl have also been explored. Table 4 shows the site and element specific moments as one passes from the XA-type structure toward the $L2_1$ structure (i.e. starting from the fully-ordered XA-type structure, sequentially swapping iron atoms in the 4c sites with vanadium atoms in the 4b sites until the fully-ordered $L2_1$ structure is reached.) It is apparent that as disorder is introduced into the system, the magnetization decreases relative to the two fully-ordered structures. A drastic change observed in the net moment between 50% XA and 25% XA is largely due to the vanadium atoms in the 4d sites now coupling antiferromagnetically to the iron atoms in the 4b and 4c sites. Note that in the XA-type structure, the vanadium atoms in the 4d sites take on a large moment of $1.88 \mu_B$ coupled ferromagnetically to the iron in the 4c sites. This vanadium moment is much greater than has been previously reported in metallic systems. For example, spin-polarized electronic structure calculations on binary FeV reveal a moment of $-0.29 \mu_B$ [18], which is consistent with what we observe for vanadium atoms in 4b and 4c sites. Polarized neutron scattering studies on bulk bcc Fe-V binary systems

have shown that vanadium can have a moment up to approximately $-3 \mu_B$, but this is only observed for very dilute concentrations of vanadium (<1 at.%) [19]. At higher vanadium concentrations the moment decreases dramatically and at 10 at.% a moment of approximately $-1 \mu_B$ is observed [20], which then falls monotonically with increasing vanadium concentration, the alloys becoming non-magnetic at 77 at.% vanadium [21]. V_2FeAl contain 50% vanadium, so one might expect a moment of about $0.4 \mu_B$ or less. We therefore believe that the calculated moment of the vanadium in the 4d sites ($1.88 \mu_B$ in fully-ordered XA structure) is overestimated in partially-disordered thin-films, and that in reality they have a moment closer in magnitude to those of the 4b and 4c sites ($0.29 \mu_B$) or to what is observed in the $L2_1$ structure ($0.86 \mu_B$). Making this assumption, we find the total moment of the XA-type structure falls in the range from $1.31 \mu_B$ to $1.88 \mu_B$ per formula unit.

Fig. 3(a) shows X-ray diffraction patterns for thin-film V_2FeAl as a function of deposition temperature. The best quality films are obtained at a temperature of $400^\circ C$, with this sample showing Laue oscillations about the (004) reflection indicating a large out-of-plane crystalline coherence length, the out-of-plane lattice parameter for this sample was found to be 583.36 pm. All subsequent data presented for ordered V_2FeAl thin-films is measured on this sample. Reciprocal space mapping of the V_2FeAl (204) and $(\bar{2}\bar{2}4)$ reflections confirm an epitaxial relationship with the $MgO(001)$ single-crystal substrate (i.e. $a = b = 595.55$ pm $\approx \sqrt{2} \cdot a_{MgO}$). The thin-films therefore show a large tetragonal distortion induced by the substrate with $c/a = 0.9795$. For the sample deposited at $700^\circ C$, it can clearly be seen that phase separation is beginning to occur with the (004) reflection showing a clear shoulder peak. Based upon the measured (002)/(004) ratio, binary FeAl was determined to be the phase responsible for this peak. Fig. 3(b) shows

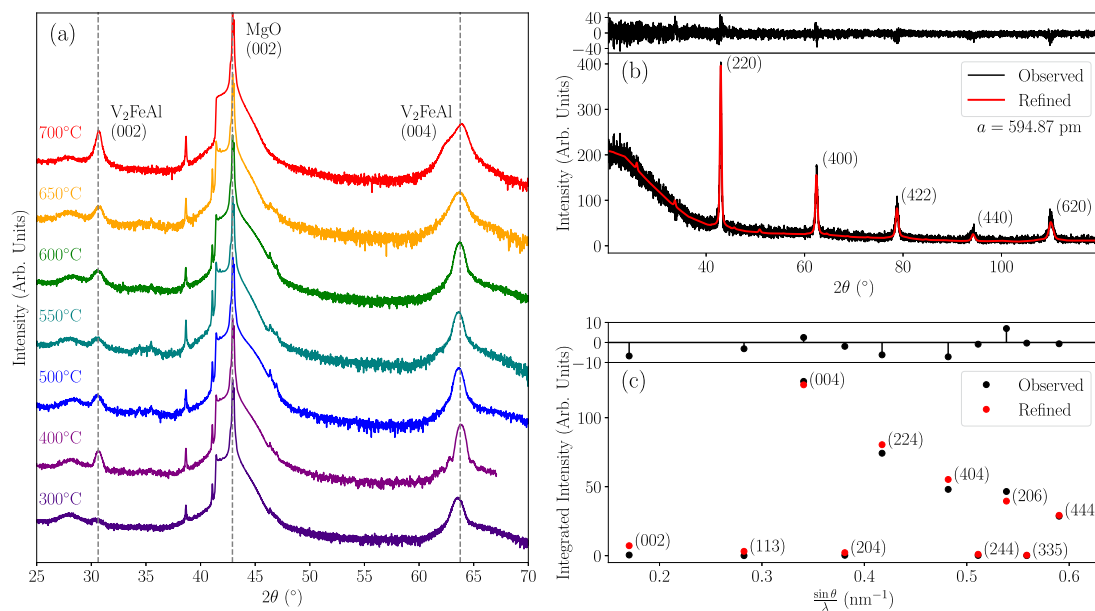


Fig. 3. (a) X-ray diffraction patterns of V_2FeAl thin-films grown at various deposition temperatures, (b) Rietveld refinement of V_2FeAl powder diffraction pattern, (c) Rietveld refinement of several integrated peak intensities captured using grazing-incidence X-ray diffraction on V_2FeAl thin-films.

the powder diffraction pattern of bulk V_2FeAl , Rietveld analysis confirms that it has the fully-disordered A2 structure (as indicated by the absence of a (002) reflection) with a lattice parameter of 594.87 pm, which corresponds well with the cubic lattice parameter predicted for the ferrimagnetic configuration of XA-type V_2FeAl , as well as with that associated by Goraus et al. [6] with the $L2_1$ structure. A number of thin-film samples deposited at lower temperatures also showed an unusually high (002)/(004) ratio, indicating the presence of FeAl, which can likely be attributed to poor epitaxial growth of V_2FeAl . These samples also contain some V_2FeAl in the fully-disordered A2 form which we observe in bulk powders. The disordered sample used for subsequent measurements was deposited at 400 °C.

ω - 2θ X-ray diffraction measurements were performed on an ordered V_2FeAl thin-film to determine the integrated intensities of ten independent reflections. After applying appropriate corrections to account for the illuminated sample area, the Lorentz polarization correction, and geometrical factors, the integrated peak intensities can be compared to those calculated from their structure factor. Rietveld refinement is performed to determine which structure type best matches the sample as shown in Fig. 3(c). The thin-film sample was closer to XA-type structure than $L2_1$ type structure, with the best fit lying somewhere between XA-type and a partially-disordered B2 structure. However, owing to the similar X-ray scattering cross-sections of vanadium and iron, there are no significant differences in intensity between reflections from the two structures. It is therefore impossible to decide the crystal structure by X-ray diffraction alone. X-ray reflectivity measurements determined the films were approximately 15 nm thick (14.70 nm thick for the ordered sample and 15.78 nm thick for the disordered). The films were all found to be smooth with RMS roughness values less than 0.5 nm, and the densities were around 5.80 g cm^{-3} (assuming full site occupancy, the nominal density is 5.83 g cm^{-3}).

The magnetic properties of both bulk and thin-film samples of V_2FeAl were measured using SQUID magnetometry. The measured magnetic moments of the thin-films were then corrected as described in the experimental section, and the anhyseretic spontaneous magnetization curves are presented in Fig. 4. The ordered thin-film shows a magnetization of approximately $1.0 \mu_B$ per formula unit at 5 K, which falls gradually to approximately $0.9 \mu_B$ per formula unit at 300 K, indicating a Curie temperature well in excess of room temperature ($T_C \sim 400 \text{ K}$). The disordered thin-film shows a magnetization of only $0.1 \mu_B$

per formula unit at 5 K, with the magnetization falling to nearly zero at room temperature ($T_C \sim 330 \text{ K}$). The fully-disordered bulk sample was a Pauli paramagnet with a volume susceptibility of $\chi_V = 2.95 \times 10^{-4}$, a smaller value than that obtained by Goraus et al. [6] ($\chi_V = 7 \times 10^{-4}$).

The XPS spectra of both ordered and disordered thin-films of V_2FeAl are presented in Fig. 5. Comparing the integrated areas of the Fe 2p, V 2p, and Al 2s peaks and applying their respective relative sensitivity factors, we find that the ordered sample contains slightly less vanadium than predicted based upon sample densities measured by XRR, but was still within 20% of the nominal composition V_2FeAl . The disordered sample was found to contain approximately 17% oxygen, significantly more than the ordered sample which contains approximately 3% oxygen. No significant contaminants other than oxygen were observed for either sample. The vanadium, iron, and aluminium peaks all appear to be mostly metallic in nature, indicating both samples are electrically conductive. Since all XPS measurements were performed directly following deposition without breaking vacuum, the excess oxygen on the disordered samples must therefore be a result of the processing conditions or contamination from the substrate.

Iron L-edge X-ray absorption spectroscopy and X-ray magnetic circular dichroism are shown in Fig. 6. The panel on the left shows the XANES signal in blue (with the background signal removed), and the XMCD signal in red. The panel on the right shows the spin and orbital moments (and their sum) obtained using the sum rules. The total iron moment for the ordered film at 10 K is found to be $1.24 \mu_B$ per iron atom, which is in good agreement with the predicted moment for the ordered XA-type structure of $1.26 \mu_B$. Comparing this to the total moment measured by SQUID of $1.0 \mu_B$ per formula unit at 5 K, we infer an average moment of $-0.12 \mu_B$ per vanadium atom, which is somewhat lower than predicted for vanadium in the 4b and 4c sites ($-0.29 \mu_B$) and much lower than the $1.88 \mu_B$ calculated for the 4d site. At a temperature of 125 K, the iron moment is reduced to $0.77 \mu_B$, whereas the total moment measured by SQUID is approximately $0.9 \mu_B$ at 100 K. Conversely, the disordered sample shows an iron moment of $1.14 \mu_B$ per atom at 10 K. Given the small total moment of $0.1 \mu_B$ at 5 K, the inferred moment on vanadium is $-0.65 \mu_B$ which decreases with temperature to $-0.33 \mu_B$ as the iron moment drops to $0.77 \mu_B$ at 125 K.

The temperature dependence of the longitudinal and transverse Hall conductivity are shown in Fig. 7(c). The transverse conductivity follows the magnetization, falling gradually from $3.64 \Omega^{-1} \text{ cm}^{-1}$ to

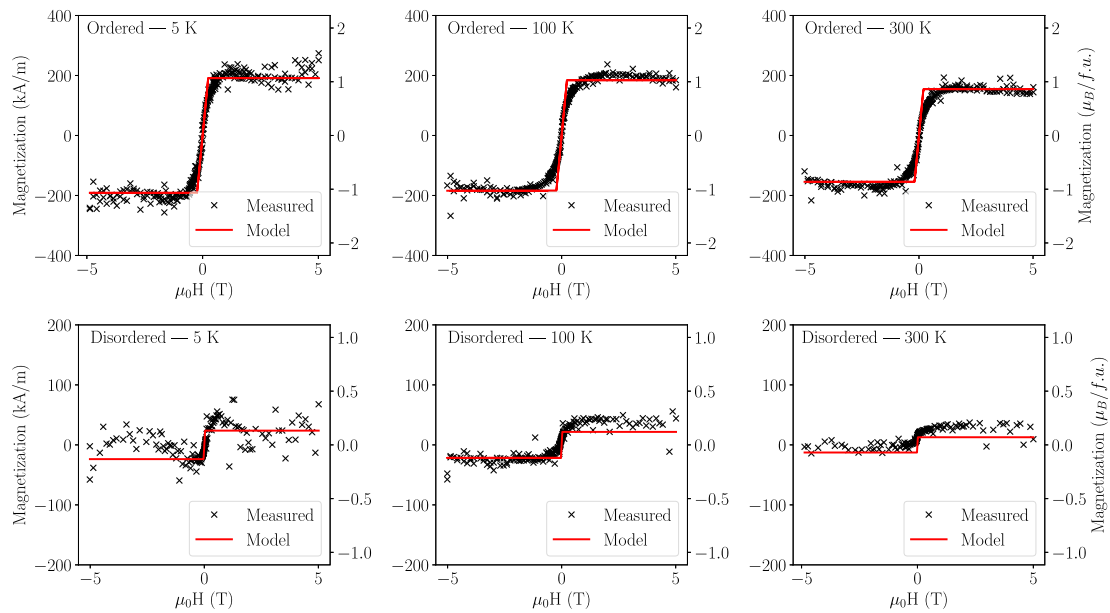


Fig. 4. Out-of-plane magnetization loops with the ferromagnetic component of the fitting model for ordered and disordered thin-films of V_2FeAl at 5 K, 100 K, and 300 K.

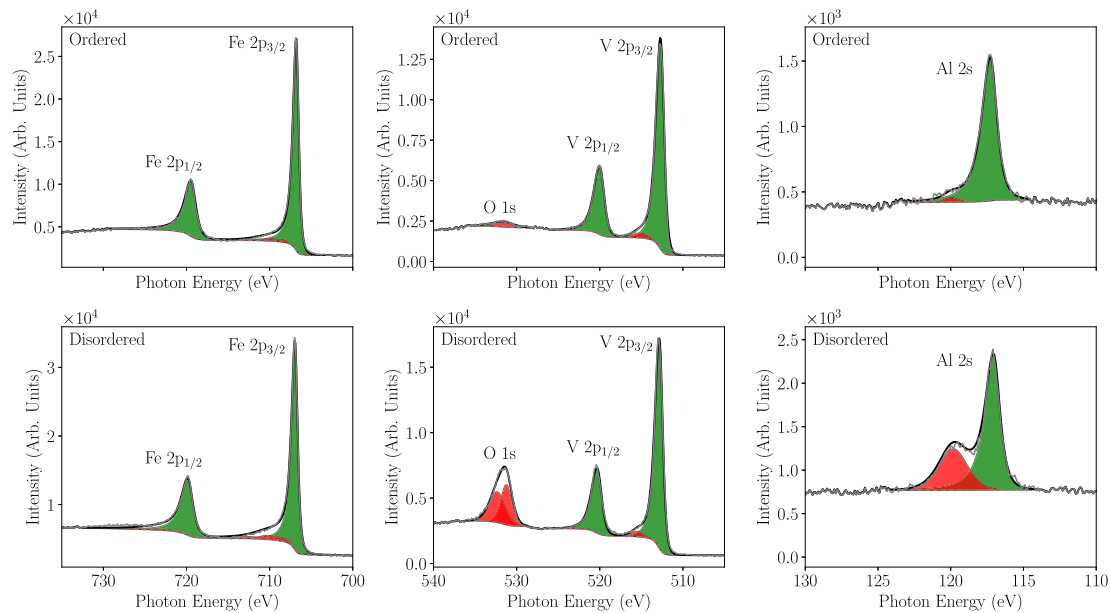


Fig. 5. XPS spectra of the Fe 2p (left), V 2p and O 1s (centre), and Al 2s peaks (right) measured on both ordered (top row) and disordered (bottom row) V_2FeAl thin films. The peaks shaded in green are metallic in nature, whereas those in red originate from oxygen or oxide species.

$2.59 \Omega^{-1} \text{cm}^{-1}$ in the temperature range 10 K to 300 K. The longitudinal conductivity is low, of order $1 \times 10^3 \Omega^{-1} \text{cm}^{-1}$, and decreases with decreasing temperature reaching a minimum of $1685 \Omega^{-1} \text{cm}^{-1}$ at approximately 50 K below which it gradually increases. This increase of conductivity with temperature indicates that the material may be semiconducting, as the anomalous Hall conductivity increases with carrier concentration. The longitudinal resistivity changes from $593.5 \mu\Omega \text{cm}$ to $501.1 \mu\Omega \text{cm}$ in this temperature range, meaning the sample does not satisfy the Mooij criterion for a metal ($100 \mu\Omega \text{cm}$ to $200 \mu\Omega \text{cm}$) [22]. However, we have found that the resistivity of bulk V_2FeAl is $267 \mu\Omega \text{cm}$, with a positive temperature coefficient of resistivity. The resistivity of our 15 nm thin-films is dominated by surface effects. We therefore conclude that V_2FeAl is not in fact semiconducting but simply a highly-resistive metallic alloy. The magnetoresistance (MR) curves presented in Fig. 7(b) show typical B^2 MR below 50 K with

a small magnitude, but show a change of sign at higher temperatures. This MR is responsible for the increase in longitudinal conductivity at low temperatures. The anomalous Hall loops shown in Fig. 7(a) show similar temperature dependence as the magnetization measured by SQUID, but the lower temperature loops are much squarer in character and have small coercivities ($<100 \text{mT}$ at 10 K) which decrease exponentially with temperature.

4. Discussion

When grown in bulk and annealed at $T_a = 650^\circ \text{C}$, V_2FeAl forms in the disordered cubic A2 structure without any spontaneous magnetization, matching the results found by Goraus et al. [6]. This is expected given the low enthalpy of formation of both ordered forms predicted by electronic structure calculations, and the entropy of disorder of $R \ln \Omega$

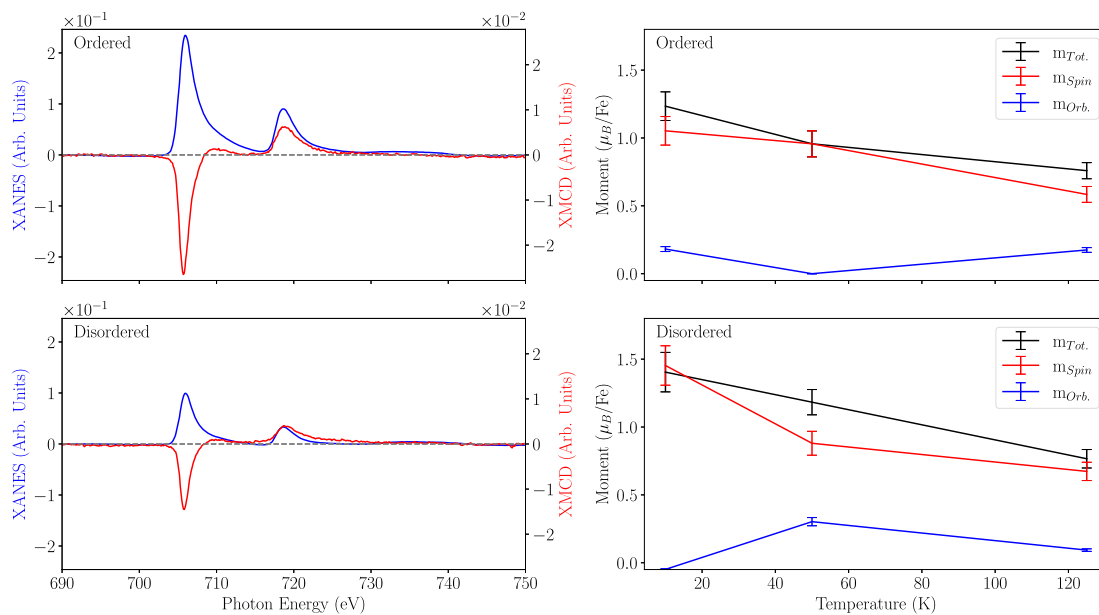


Fig. 6. The X-ray absorption spectrum (with the background removed) and the dichroic XMCD signal measured on an ordered and disordered thin-film of V_2FeAl (left), and the spin, orbital and total magnetic moments calculated using the sum rules as a function of temperature (right).

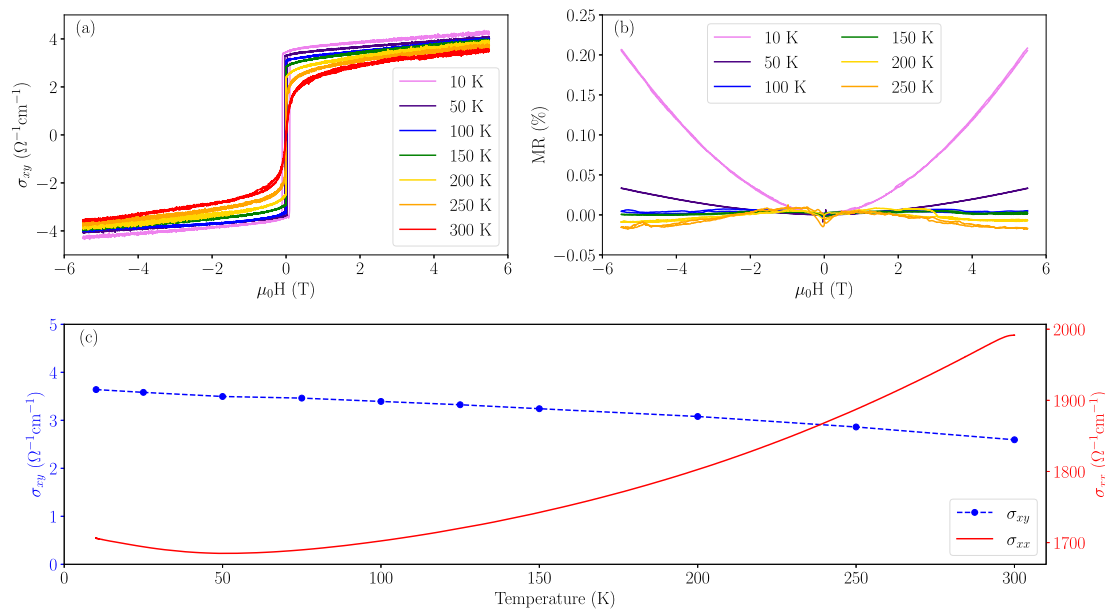


Fig. 7. (a) Hall conductivity field loops at various temperatures, (b) magnetoresistance at various temperatures, (c) Hall conductivity (blue) and longitudinal conductivity (red) as a function of temperature measured in an applied field of 5.5 T.

per mole (R is the universal gas constant, Ω the number of possible configurations of the system, in this case $\Omega = 12$), which reduces the free energy by $RT_a \ln \Omega = 19 \text{ kJ mol}^{-1}$ at the annealing temperature of 923 K. Contrast this to the calculated total energy difference per atom shown in Fig. 2, which shows an energy difference of 159 meV between the ferrimagnetic $L2_1$ and XA-type structures corresponding to a value of approximately 15 kJ mol^{-1} . The energy associated with disordering the system is therefore of the same order of magnitude as the energy difference between the different structures, indicating that formation of fully-ordered alloys is unlikely.

Bulk V_2FeAl may be regarded as a high-entropy alloy like $CrVTiAl$ quaternaries that are also Pauli paramagnets [23]. However, when deposited in thin-film form on an appropriate substrate, in our case $MgO(001)$, the induced tetragonal distortion stabilizes a more highly ordered form of V_2FeAl , allowing for ferrimagnetic ordering between

the iron and vanadium atoms, as opposed to the paramagnetic behaviour observed in bulk samples. These ordered thin-film samples show a structure which lies somewhere between the fully-ordered XA-type and the partially ordered B2 structure. In all cases, XA-type structure appears to be preferred to $L2_1$ structure, which corroborates the predicted stability of the different configurations shown in Fig. 2. X-ray photoelectron spectroscopy indicates that the disordered thin-films have a much higher concentration of surface oxygen than the ordered films. It is unclear whether this oxygen is the result of contamination during the deposition process, or diffusion from poor quality MgO substrates. The larger fraction of oxide species in the disordered sample means there will be less electrons available in the conduction band as they are bonding with the oxygen, and as a result a charge transfer between the iron and the other elements leaving more iron 3d core holes. This explains the approximately 40% more holes in the

disordered sample which was determined from the magnitude of the XANES edge-jumps. The magnetic properties of the thin-film samples is highly dependent upon their ordering, with the ordered thin-film sample showing a saturation magnetization an order of magnitude greater than the disordered film at 5 K as well as a higher Curie temperature.

It is apparent that disorder has a significant effect on the magnetic properties of V_2FeAl . The ordered thin-film at low temperature, which shows a total moment of $1.0 \mu_B$ per formula unit and an iron moment of $1.24 \mu_B$ per atom, from which we infer a vanadium moment of $-0.12 \mu_B$ per atom. Comparing this to the calculated moments presented in Table 4, we find the iron moment to be in good agreement with the predicted moment for a fully-ordered XA-type structure. At the same time, there is no indication of a large vanadium moment, and the measured moments are also slightly lower than those predicted for vanadium in the $4b$ and $4c$ sites. This is consistent with our assumption that DFT overestimates the vanadium moments in this system. Conversely, the disordered thin-film sample shows a low-temperature total moment of $0.1 \mu_B$ per formula unit and an iron moment of $1.40 \mu_B$ per atom, from which we infer a vanadium moment of about $-0.65 \mu_B$. The larger iron and vanadium moments and lower total moment relative to the ordered sample is consistent with what is observed in the DFT results as disorder is introduced to the system. Comparison with Table 4 suggests that the disordered sample is approximately 25% XA-type structure.

5. Conclusion

Spontaneous magnetism in V_2FeAl depends critically on establishing some ordering of the atomic constituents on the four face-centred cubic crystallographic sites of the Heusler structure. Our electronic structure calculations show that the energy difference between the $L2_1$ and XA-type ordered structure is approximately 15 kJ mol^{-1} . Annealed bulk material with a high-entropy, fully-disordered A2 structure is found experimentally and it is a Pauli paramagnet. Tetragonally-distorted thin-films grown on MgO substrates exhibit spontaneous magnetism that depends on the degree of disorder and oxidation. Substrate templated thin-film samples with tetragonal distortion can stabilize a partly XA-ordered V_2FeAl structure which shows a spontaneous magnetization with moments on both iron and vanadium. The measured iron moments match well with DFT predictions, but the total moment is lower than predicted for a fully-ordered XA-type structure. Based upon comparison to the binary FeV system with similar vanadium concentrations, we accredit this discrepancy to an overestimation of the moments of vanadium in the $4d$ sites when they are not fully occupied by vanadium. The formation of the metastable ordered structure appears to be hindered by the presence of oxygen in the thin-film. We believe that in reality the $4d$ vanadium moments are closer to those predicted for the $4b$ and $4c$ sites, resulting in a lower total moment. A drawback of electronic structure calculations based on small superstructures is that to capture the nuances of disorder in imperfectly-ordered alloys they would need to consider much larger unit cells than that of the basic Heusler structure.

Declaration of competing interest

The authors declare that they have no known competing financial interests or personal relationships that could have appeared to influence the work reported in this paper.

Acknowledgements

The authors acknowledge financial support from Science Foundation Ireland through contract 16/IA/4534 ZEMS. The authors acknowledge the support of Dr. Alevtina Smekhova of Helmholtz-Zentrum Berlin for performing X-ray absorption and dichroism measurements.

References

- [1] T. Graf, C. Felser, S. Parkin, Simple rules for the understanding of Heusler compounds, *Prog. Solid State Chem.* 39 (1) (2011) 1–50, <http://dx.doi.org/10.1016/j.progsolidstchem.2011.02.001>, URL <https://www.sciencedirect.com/science/article/pii/S0079678611000021>.
- [2] K. Inomata, N. Ikeda, N. Tezuka, R. Goto, S. Sugimoto, M. Wojcik, E. Jedryka, Highly spin-polarized materials and devices for spintronics, *Sci. Technol. Adv. Mater.* 9 (2008) 014101, <http://dx.doi.org/10.1088/1468-6996/9/1/014101>.
- [3] C. Palmstrom, Heusler compounds and spintronics, *Prog. Cryst. Growth Charact. Mater.* 62 (2) (2016) 371, <http://dx.doi.org/10.1016/j.pcrysgrow.2016.04.020>, URL <https://www.sciencedirect.com/science/article/pii/S0960897416300237>.
- [4] J. Hu, S. Granville, H. Yu, Spin-dependent thermoelectric transport in Cobalt-based Heusler alloys, *Ann. Physics* 532 (11) (2020) 1900456, <http://dx.doi.org/10.1002/andp.201900456>, URL <https://onlinelibrary.wiley.com/doi/abs/10.1002/andp.201900456>.
- [5] V. Chernenko, M. Ohtsuka, M. Kohl, V. Khovailo, T. Takagi, Transformation behavior of Ni–Mn–Ga thin films, *Smart Mater. Struct.* 14 (5) (2005) S245, <http://dx.doi.org/10.1088/0964-1726/14/5/012>.
- [6] J. Gorau, M. Fijałkowski, J. Czerniewski, W. Gumulak, Magnetic properties of V_2MnGa , V_2MnAl , V_2FeGa and V_2FeAl , *J. Magn. Magn. Mater.* 585 (2023) 171103, <http://dx.doi.org/10.1016/j.jmmm.2023.171103>, URL <https://www.sciencedirect.com/science/article/pii/S0304885323007539>.
- [7] R.E. Watson, M. Weinert, Transition-metal aluminide formation: Ti, V, Fe, and Ni aluminides, *Phys. Rev. B* 58 (1998) 5981, <http://dx.doi.org/10.1103/PhysRevB.58.5981>, URL <https://link.aps.org/doi/10.1103/PhysRevB.58.5981>.
- [8] M. Kumar, T. Nautiyal, S. Auluck, First-principles calculations of electronic and optical properties of $Fe_{3-x}V_xAl$ ($x = 0-3$) compounds, *J. Phys.: Condens. Matter* 21 (44) (2009) 446001, <http://dx.doi.org/10.1088/0953-8984/21/44/446001>.
- [9] X. Zhang, X. Dai, G. Chen, H. Liu, H. Luo, Y. Li, W. Wang, G. Wu, G. Liu, First-principle study for full-Heusler compounds V_2YAl ($Y=V, Cr, Mn, Fe, Co, Ni$) and a discussion to Slater–Pauling rule, *Comput. Mater. Sci.* (ISSN: 0927-0256) 59 (2012) 1–5, <http://dx.doi.org/10.1016/j.commatsci.2012.02.014>, URL <https://www.sciencedirect.com/science/article/pii/S0927025612000808>.
- [10] S. Skafrouros, K. Özdoğan, E. Şaşıoğlu, I. Galanakis, Generalized Slater–Pauling rule for the inverse Heusler compounds, *Phys. Rev. B* 87 (2013) 024420, <http://dx.doi.org/10.1103/PhysRevB.87.024420>, URL <https://link.aps.org/doi/10.1103/PhysRevB.87.024420>.
- [11] M. Björck, G. Andersson, GenX: an extensible X-ray reflectivity refinement program utilizing differential evolution, *J. Appl. Crystallogr.* 40 (2007) 1174, <http://dx.doi.org/10.1107/S0021889807045086>.
- [12] J. Rodriguez-Carvajal, FULLPROF: a program for rietveld refinement and pattern matching analysis, in: *Satellite Meeting on Powder Diffraction of the XV Congress of the IUCr*, Vol. 127, Toulouse, France: [sn], 1990.
- [13] M. Venkatesan, P. Kavle, S.B. Porter, K. Ackland, J.M.D. Coey, Magnetic analysis of polar and nonpolar oxide substrates, *IEEE Trans. Magn.* 50 (11) (2014) 1, <http://dx.doi.org/10.1109/TMAG.2014.2324899>, URL <https://ieeexplore.ieee.org/abstract/document/6971312>.
- [14] C.T. Chen, Y.U. Idzerda, H.-J. Lin, N.V. Smith, G. Meigs, E. Chaban, G.H. Ho, E. Pellegrin, F. Sette, Experimental confirmation of the X-Ray magnetic circular dichroism sum rules for Iron and Cobalt, *Phys. Rev. Lett.* 75 (1995) 152, <http://dx.doi.org/10.1103/PhysRevLett.75.152>, URL <https://link.aps.org/doi/10.1103/PhysRevLett.75.152>.
- [15] T. Ozaki, H. Kino, Numerical atomic basis orbitals from H to Kr, *Phys. Rev. B* 69 (2004) 195113, <http://dx.doi.org/10.1103/PhysRevB.69.195113>, URL <https://link.aps.org/doi/10.1103/PhysRevB.69.195113>.
- [16] J. Perdew, K. Burke, M. Ernzerhof, Generalized gradient approximation made simple, *Phys. Rev. Lett.* 77 (1996) 3865–3868, <http://dx.doi.org/10.1103/PhysRevLett.77.3865>, URL <https://link.aps.org/doi/10.1103/PhysRevLett.77.3865>.
- [17] R. D. L. Bainsla, A. Alam, K. Suresh, Spin-gapless semiconductors: Fundamental and applied aspects, *J. Appl. Phys.* 128 (22) (2020) 220902, <http://dx.doi.org/10.1063/5.0028918>.
- [18] R. Jordan, X. Wang, A. Begley, S. Qiu, Y. Liu, Correspondence between the Fe 3s photoemission line-shape and the Fe local moment in Fe-V alloys, *Solid State Commun.* 78 (12) (1991) 1045–1048, [http://dx.doi.org/10.1016/0038-1098\(91\)90126-G](http://dx.doi.org/10.1016/0038-1098(91)90126-G), URL <https://www.sciencedirect.com/science/article/pii/003810989190126G>.
- [19] F. Kajzar, G. Parette, Magnetic-moment distribution and environmental effects in dilute iron-based alloy with V, Cr, and Mn impurities, *Phys. Rev. B* 22 (1980) 5471, <http://dx.doi.org/10.1103/PhysRevB.22.5471>, URL <https://link.aps.org/doi/10.1103/PhysRevB.22.5471>.
- [20] I. Mirebeau, G. Parette, J. Cable, Polarised neutron study of iron-vanadium alloys, *J. Phys. F: Met. Phys.* 17 (1) (1987) 191, <http://dx.doi.org/10.1088/0305-4608/17/1/024>.
- [21] D.J. Lam, D.O. Van Ostenburg, M.V. Nevitt, H.D. Trapp, D.W. Pracht, Magnetic susceptibilities and nuclear magnetic resonance measurements in V-Fe alloys, *Phys. Rev.* 131 (1963) 1428–1433, <http://dx.doi.org/10.1103/PhysRev.131.1428>, URL <https://link.aps.org/doi/10.1103/PhysRev.131.1428>.

- [22] J.H. Mooij, Electrical conduction in concentrated disordered transition metal alloys, *Phys. Status Solidi A* 17 (2) (1973) 521–530, <http://dx.doi.org/10.1002/pssa.2210170217>, arXiv:<https://onlinelibrary.wiley.com/doi/pdf/10.1002/pssa.2210170217> URL <https://onlinelibrary.wiley.com/doi/abs/10.1002/pssa.2210170217>.
- [23] R. Zhang, Z. Gercsi, M. Venkatesan, K. Rode, J.M.D. Coey, Pauli paramagnetism of cubic V_3Al , $CrVTiAl$, and related 18-electron Heusler compounds with a group-13 element, *Phys. Rev. B* 103 (2021) 174407, <http://dx.doi.org/10.1103/PhysRevB.103.174407>, URL <https://link.aps.org/doi/10.1103/PhysRevB.103.174407>.